Environmental Science & Technology

Article

pubs.acs.org/est

Photochemical Transformation of Graphene Oxide in Sunlight

Wen-Che Hou,*[,†,‡] Indranil Chowdhury,[†] David G. Goodwin, Jr.,[§] W. Matthew Henderson,[⊥] D. Howard Fairbrother,[§] Dermont Bouchard,[⊥] and Richard G. Zepp*[,⊥]

[†]National Research Council Associate, National Exposure Research Laboratory, Ecosystems Research Division, U.S. Environmental Protection Agency, Athens, Georgia 30605, United States

[‡]Department of Environmental Engineering, National Cheng Kung University, Tainan City 70101, Taiwan

[§]Department of Chemistry, Johns Hopkins University, Baltimore, Maryland 21218, United States

[⊥]National Exposure Research Laboratory, Ecosystems Research Division, U.S. Environmental Protection Agency, Athens, Georgia 30605, United States

Supporting Information

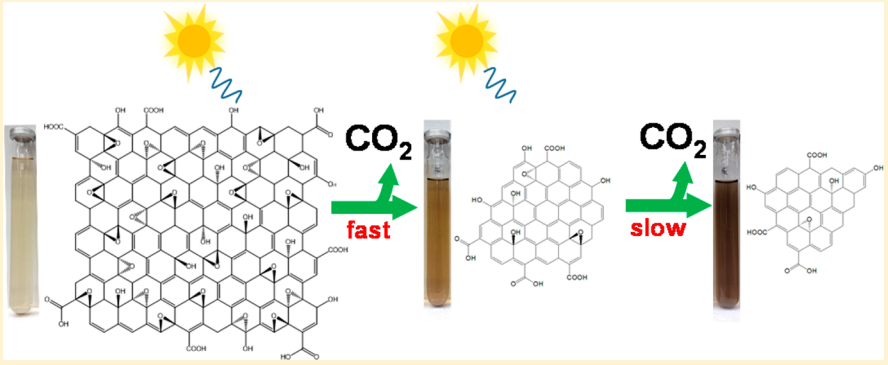

ABSTRACT: Graphene oxide (GO) is promising in scalable production and has useful properties that include semiconducting behavior, catalytic reactivity, and aqueous dispersibility. In this study, we investigated the photochemical fate of GO under environmentally relevant sunlight conditions. The results indicate that GO readily photoreacts under simulated sunlight with the potential involvement of electron−hole pair creation. GO was shown to photodisproportionate to CO_2, reduced materials similar to reduced GO (rGO) that are fragmented compared to the starting material, and low molecular-weight (LMW) species. Kinetic studies show that the rate of the initially rapid photoreaction of GO is insensitive to the dissolved oxygen content. In contrast, at longer time points (>10 h), the presence of dissolved oxygen led to a greater production of CO_2 than the same GO material under N_2-saturated conditions. Regardless, the rGO species themselves persist after extended irradiation equivalent to 2 months in natural sunlight, even in the presence of dissolved oxygen. Overall, our findings indicate that GO phototransforms rapidly under sunlight exposure, resulting in chemically reduced and persistent photoproducts that are likely to exhibit transport and toxic properties unique from parent GO.

INTRODUCTION

Graphene oxide (GO) is an important precursor to graphene, a one-atom thick, two-dimensional nanomaterial made of sp^2-hybridized carbon that has received unprecedented attention as a result of its fundamental properties and broad applications.[1,2] The hydrophobic nature and absence of a bandgap, however, limit graphene's utility in water-based applications (e.g., biomedicines), as well as in light-emitting electronics and photocatalysis.[3,4] GO is a structural analog to graphene with added functionalities such as epoxy, hydroxyl, carbonyl, and carboxyl groups covalently bound on the basal planes (for epoxy and hydroxyl groups) or the edges (for carbonyl and carboxyl groups).[4,5] Beyond structural variation, however, GO has other promising characteristics distinct from graphene: for example, in addition to enhanced aqueous dispersibility, GO is more likely to be made in large batches due to its scalable production process involving oxidative exfoliation of graphite in aqueous solutions containing concentrated acids and oxidants.[4] The oxygen groups are the basis for further covalent attachment of smaller molecules or polymers to GO.[4] Although extensive oxidation destroys the sp^2-hybridized carbon network, rendering GO electrically insulating, GO can be readily reduced by chemical, thermal, electrochemical, photocatalytic, or microbial reactions to produce rGO for recovery of electron-conducting capabilities.[6−9]

Recent studies examined potential risks to ecosystems posed by graphene and GO. Several studies have shown that graphene

Received: September 25, 2014
Revised: February 8, 2015
Accepted: February 11, 2015
Published: February 11, 2015

DOI: 10.1021/es5047155
Environ. Sci. Technol. 2015, 49, 3435−3443

Scheme 1. Pathways of GO Phototransformation in Sunlight

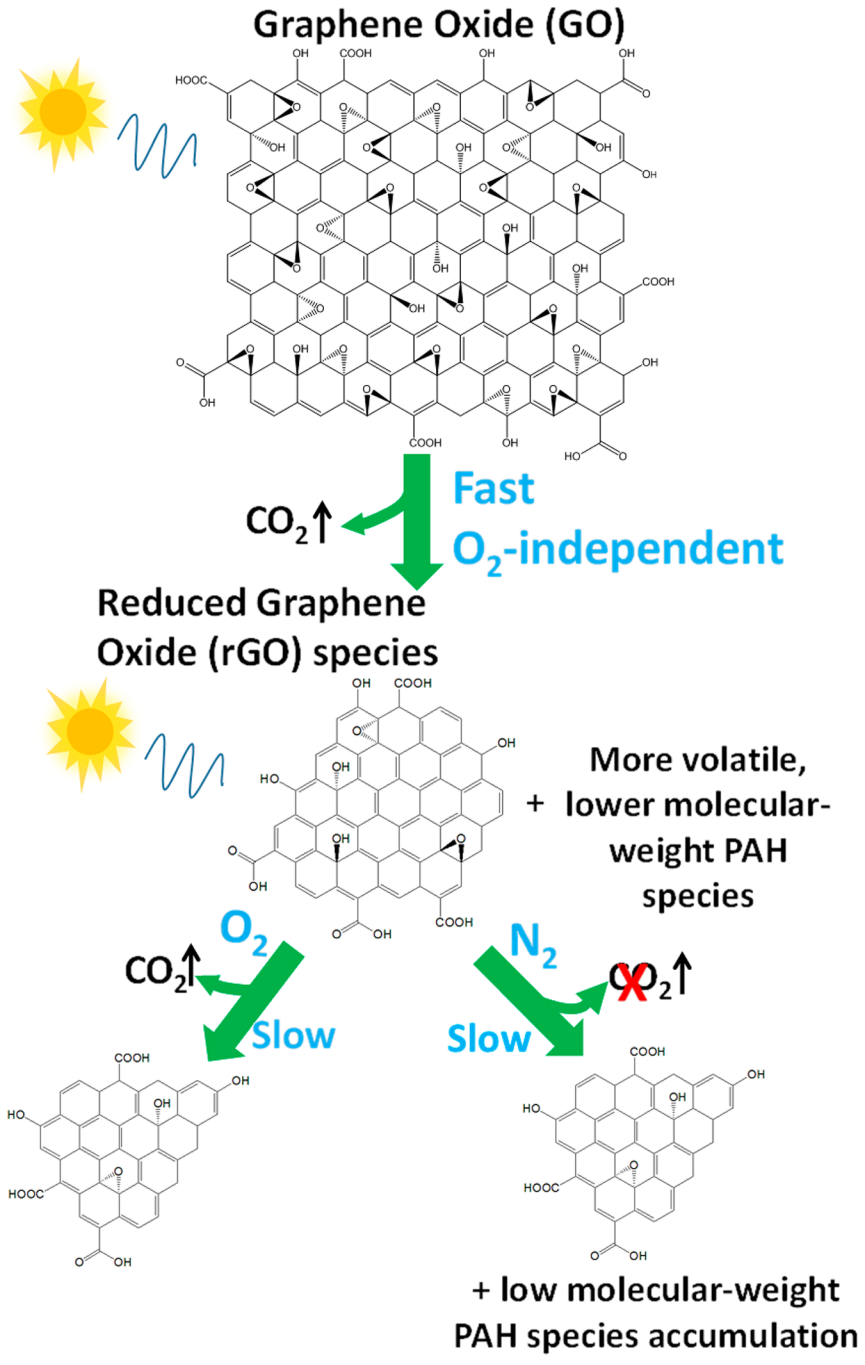

and its derivatives exhibit cytotoxicity to Gram-negative and Gram-positive bacteria and to wastewater sludge microorganisms.[10−13] Begum et al. indicated that GO is phytotoxic to many edible plants;[14] additionally, Guo et al. showed that *Daphnia* can uptake radio-labeled GO to 1% of their dry weight and that adult *Daphnia* probably transfer GO material to their offspring.[15] On the other hand, research on the fate and transport of GO is limited. Studies indicate that GO could be stable in natural surface waters and that it tends to aggregate and deposit on silica surfaces in groundwater systems, with the possibility of remobilization.[16−20] These results suggest that GO could be suspended and transported in water columns for some time, where phototransformation processes mediated by sunlight would become important. Work on the transformation of GO in the environment is basically nonexistent, with just a few studies showing that enzymatic reactions may occur;[21,22] this highlights the need for research on the transformation fate of graphene and its derivatives.

Studies of GO photoreactions are just starting to emerge. It has been shown that GO can be photochemically or thermally reduced with exposure to high-energy UV-C and laser light.[23−25] However, the wavelengths and/or strong laser light intensity of light sources used in existing studies are not present in the solar spectrum and therefore may not be predictive of photoreactions occurring under natural sunlight conditions. For example, a recent study shows that UV-C irradiation of natural organic matter induces the photoproduction of highly reactive hydroxyl radical at orders of magnitude higher than under solar

DOI: 10.1021/es5047155
Environ. Sci. Technol. 2015, 49, 3435−3443

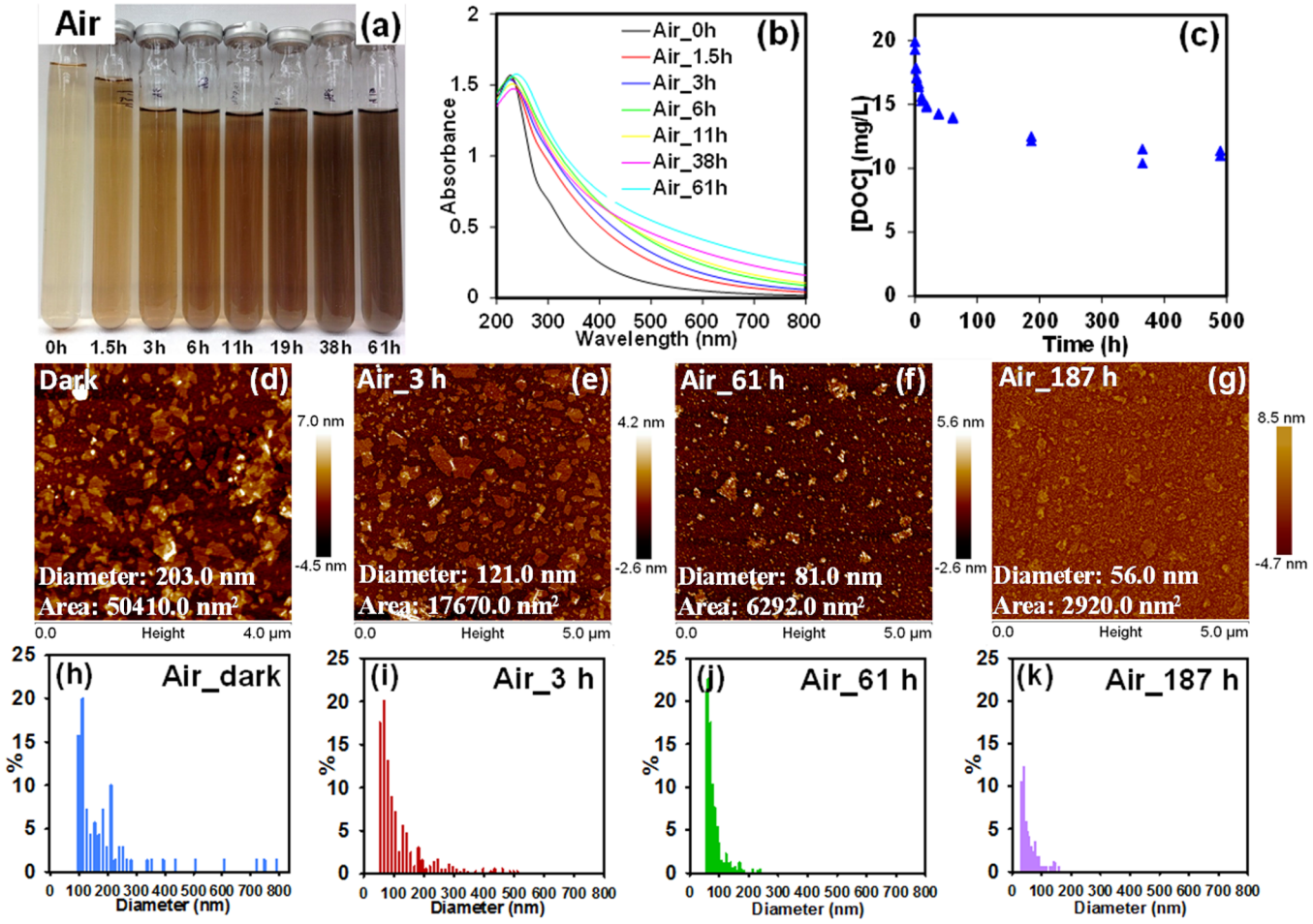

Figure 1. Phototransformation of graphene oxide (GO) in sunlight, showing (a) the photograph of air-equilibrated samples before and after sunlight exposure, (b) the UV−visible absorbance and (c) DOC of the same samples, and (d−g) AFM images of GO before and after irradiation. Data presented in panels h−k indicate size distributions of respective samples. The diameters and areas indicated in the AFM images are mean equivalent diameters and mean areal sizes of individual GO nanosheets.

irradiation.[26] As will become clear in this paper, our findings indicate that the photoreduction behavior of GO in sunlight is distinct from that under UV-C irradiation in terms of rate and reaction order. We measured the photoreaction kinetics by monitoring the CO_2 evolution and corresponding changes in the oxygen-containing functionalities of GO under air- versus N_2-equilibrated conditions. Additionally, the phototransformed GO under sunlight conditions was found to contain a significant level of remaining oxygen relative to photo-transformed GO under UV-C irradiation conditions. Photo-products were characterized by a range of complementary analytical techniques including mass spectrometry, atomic force microscopy (AFM), X-ray photoelectron spectroscopy (XPS), UV−visible absorbance, as well as infrared, Raman, and fluorescence spectroscopies. The dissolved oxygen level was also varied and long-term irradiation times were carried out for up to ∼500 h, equivalent to ∼2 months under natural sunlight, to assess the photochemical fate of GO under various environmentally relevant conditions. These aspects were not considered in earlier studies that were not designed to study the environmental fate of GO.

In summary, our collective findings indicate that GO initially undergoes a fast photoreaction (<10 h), followed by a period when intermediate photoproducts derived from initial irradiation react more slowly in an O_2-dependent manner. The intermediate photoproducts are characterized to have reduced sizes and decreased oxygen functionalities and include LMW species that exhibit distinct photoreactivity from parent GO. Ultimately, photoreactivity of GO under both air- and N_2-saturated conditions results in products only slowly transformed by sunlight exposure. The overall phototransformations of GO are summarized in Scheme 1.

MATERIALS AND METHODS

Materials. The GO sample was obtained from Cheap Tubes Inc. (Brattleboro, VT) in a 2 mg/mL dispersion in pure water. According to the supplier, the GO material was manufactured by the modified Hummer's method.[27] All other chemicals were used as supplied from Sigma-Aldrich (St. Louis, MO). All aqueous samples were prepared with water purified using an Aqua Solutions 2121BL system (≥18.0 MΩ).

Irradiation. The sunlight experiments were carried out in an Atlas SunTest CPS+ solar simulator equipped with a 1 kW xenon arc lamp. Reaction vessels were 24 mL quartz tubes, to which 20 mL of reaction solution was added. Samples were not pH-buffered, but the pH was monitored before and after irradiation and stayed in the range of 4.0−4.3. The sample tubes were sealed with open-top caps lined with gastight PTFE septa, submerged in a thermostated water bath (25 °C) during irradiation. The incident light intensity at the tube surface,

DOI: 10.1021/es5047155
Environ. Sci. Technol. 2015, 49, 3435−3443

summed from 290 to 700 nm, was 0.065 W/cm^2. For kinetic studies, a series of tubes were prepared for irradiation. At specific time periods during irradiation, one tube was removed from the reactor and sacrificed for chemical analysis. Dark control tubes were covered by aluminum foil and irradiated concurrently and analyzed in the same manner. Therefore, any differences observed could be attributed solely to light irradiation. We performed experiments using duplicate samples. Procedures for dissolved oxygen level studies, CO_2 measurements, and photoproduct preparation are presented in the Supporting Information.

Characterization of GO Photoproducts. Procedures for characterizing GO photoproducts including mass spectrometry, UV−visible absorbance, dissolved organic carbon (DOC) analysis, fluorescence, X-ray photoelectron spectroscopy (XPS), attenuated total reflectance-infrared spectroscopy (ATR-IR), dynamic light scattering (DLS), and atomic force microscopy (AFM) are presented in the Supporting Information.

RESULTS AND DISCUSSION

GO Characterizations. The AFM image analysis indicates that the as-received, pristine GO nanosheets have a mean areal size of ~50 000 nm^2, mean diameter of 203 nm, and thickness in the range of 0.7−1.2 nm. The GO material is strongly oxidized with an oxygen-to-carbon atom ratio (O/C) of 0.6. XPS results are similar to previous studies in which GO contains the same oxygen-containing functional groups, specifically 43.5% C—OH and C—O—C, 2.4% C═O, and 6.9% O—C═O for the GO used in this study.[7,28] Raman analysis indicates a large D (1354 cm^{-1})-to-G (1595 cm^{-1}) band intensity ratio (I_D/I_G) of 0.85 for the as-received GO sample characteristic of strongly oxidized graphitic carbon materials.[29] The UV−visible light absorbance spectrum of pristine GO is featureless within the solar spectrum (280−800 nm), with absorbance increasing monotonically as wavelength decreases.[28,30]

Phototransformations of GO. Figure 1 shows that sunlight exposure darkens the color of air-saturated GO samples (Figure 1a), increases the UV−visible absorbance above 280 nm (Figures 1b and S1, Supporting Information), and reduces the DOC content (Figure 1c) as irradiation time increases, indicating GO is photochemically altered and that light-absorbing photoproducts are formed. AFM images (Figure 1d−g) show that irradiated GO nanoplatelets were broken into fragments: for example, the mean equivalent diameters and mean areal sizes of individual nanoplatelets fragmented from 203.0 and 50 410.0 nm^2 to 56.0 and 2920.0 nm^2, respectively, after 187 h of irradiation in air-saturated samples. Thus, the size distribution of irradiated GO strongly shifts to a smaller range (Figure 1h−k).

Inorganic carbon (IC) content (i.e., CO_2) increases with increased irradiation time (see Figure 2a), indicating that sunlight exposure photochemically converts GO to CO_2. The CO_2 formation is concurrent with the loss of DOC (Figure 1c). The IC measured at the plateau is approximately 6 mg/L. Although we also examined the formation of CO, its concentration was negligible in our system. Interestingly, the concurrent formations of CO_2 and chemically reduced photoproducts (see the Photoproduct Characterizations section) indicate that GO photoreactivity results in its disproportionation, a redox reaction in which a species is simultaneously reduced and oxidized to form two different

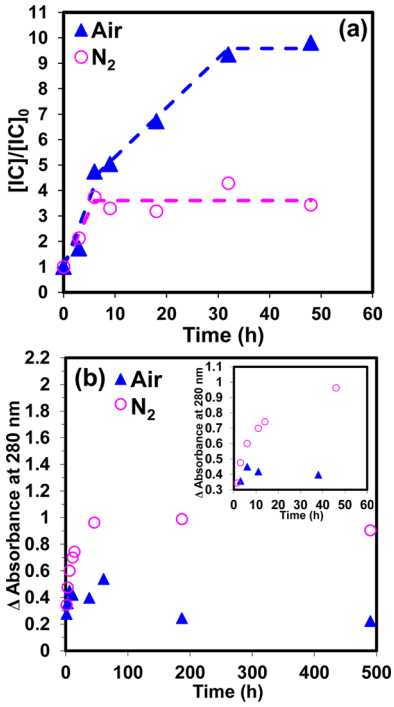

Figure 2. Effect of O_2 level on (a) CO_2 formation, and (b) Δ absorbance at 280 nm of air- and N_2-saturated samples irradiated under simulated solar light. Lines in panel a are used to guide the eyes.

products. The photochemical mineralization of GO to CO_2 was incomplete because formation of CO_2 (see Figure 2a) and loss of DOC (Figure 1c) reached a plateau after 50 h of irradiation. For irradiation times in excess of 50 h the DOC (Figure 1c), light absorbance (Figure S1a, Supporting Information), and hydrodynamic size (Figure S2, Supporting Information) remained unchanged even after extended irradiation times of ~500 h, equivalent to two months under natural sunlight.

Photoproduct Characterizations. LMW species formation was assessed to determine their involvement in the photochemical conversion of GO to CO_2. The mass spectra presented in Figure 3a indicate the occurrence of LMW species with m/z ranging from ~60−730 in air-equilibrated samples after 11 h of irradiation. With continued irradiation, the abundance of these species increased (Figure 3b) and additional species in the lower m/z range (i.e., 200−500) were present (Figure 3c). The tentative assignments of the LMW species are hydroxylated and/or carboxylated polycyclic aromatic hydrocarbon (PAH) compounds, as shown in Figure 3. Although the assignments are preliminary, and additional work is needed, the formation of oxygenated PAH species is consistent with previous work in which GO transformation was driven by a photo-Fenton reaction.[31,32] There has been no known prior study trying to identify or measure LMW species formed under irradiation without added catalysts. Our study is likely the first to report their occurrence under direct photolysis conditions.

Additional characterization using XPS, ATR-IR, and Raman spectroscopic analyses of GO photoproducts, prepared by freeze-drying irradiated aqueous samples, are presented in Figures 4 and S3, Supporting Information (for ATR-IR and Raman). These characterizations are more indicative of the larger fragment materials of GO other than LMW compounds, as LMW compounds would have evaporated during freeze-

DOI: 10.1021/es5047155
Environ. Sci. Technol. 2015, 49, 3435−3443

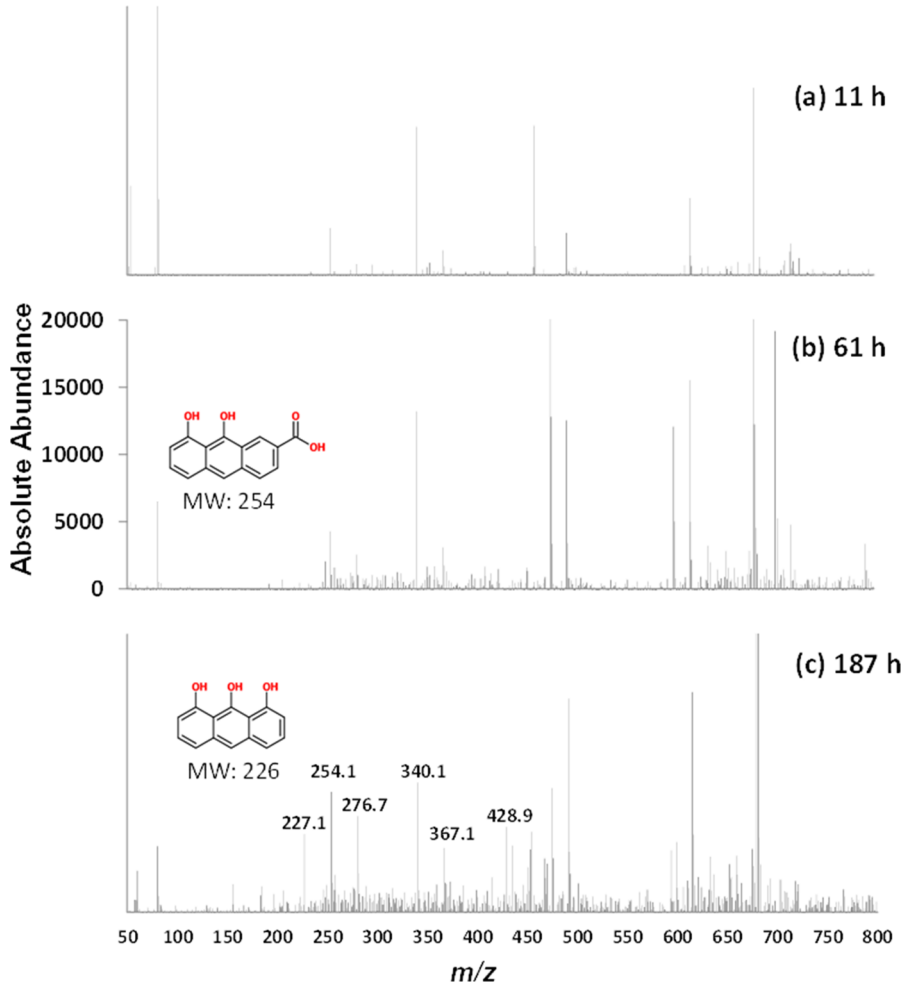

Figure 3. Mass spectra of (a) 11 h, (b) 61 h, and (c) 187 h irradiated samples under air-equilibrated conditions. The average spectral response of the dark control GO sample was subtracted from each time point. All spectra are plotted on the same scale and proposed structures for m/z of 226 and 254 are presented.

drying or under ultrahigh vacuum conditions during XPS analyses. The XPS results (Figure 4) indicate irradiated GO samples are strongly reduced, forming photoproducts with decreased concentrations of oxygen-containing functionalities (including C—O, C═O, and O—C═O groups) from 52% to 27%; conversely, their graphitic carbon contents (including C—C, C═C, and C—H groups) increased from 46% to 73% after 187 h of sunlight exposure. Very similar trends and percent oxygen functional groups were observed for samples irradiated in N_2-purged systems, as shown with detailed XPS, ATR-IR, and Raman analyses in Figure S4 (Supporting Information).

The strong reduction in oxygen-containing functionalities observed by XPS suggests the photoreactive sites mainly lie on the basal plane where epoxy and hydroxyl groups are the dominant functionalities.[4,5] The ATR-IR results (Figure S3a, Supporting Information) are generally consistent with the XPS data, indicating a strong reduction in C—OH (broad peak centered at 3250 cm^{-1}) and C—O—C (sharp peak centered at 1020 cm^{-1}) features while the two peaks in the C═O stretching region (1500−1840 cm^{-1}) remain essentially unchanged.

The Raman spectra of both air- and N_2-saturated samples (Figures S3b and S4c, Supporting Information) indicate a small increase in the I_D/I_G ratio during the initial period of irradiation (<10 h), which achieves a constant value with continued light exposure (Figure S5, Supporting Information). This contrasts with observed reduction of the oxygen-containing functionalities (i.e., defect sites), but is consistent with Raman data on the reduction of GO by hydrazine.[7] This can be understood if we recognize that in the Raman spectra of the parent GO, the D-band arises principally from the sp^3 carbon atoms associated with oxygen-containing functional groups. Photolysis of GO leads not only to reduction of carbon atoms associated with oxygen-containing functional groups but also to significant degree of fragmentation. This process significantly increases the number of GO edges or "border defects", which have been shown to contribute to the D-band intensity (I_D) due to disruption of the macroscopic aromatic network at these locations.[7,33−36]

Kinetics. The time courses of photoreduction (as evaluated by the decrease in O/C) and the functional group changes in the GO samples are presented in Figure 5. The overall rate of decrease in the O/C ratio for air-equilibrated samples is not well-described by the pseudo-first-order kinetics (R^2 = 0.61) (see Figure 5a). The initial rate (<11 h) of reduction as measured by the O/C ratio does, however, appear to be relatively first-order (R^2 = 0.89) with a rate constant of 0.017 ± 0.018 h^{-1} [error indicates 95% confidence interval (CI)], but this rate decreases by more than an order of magnitude to

DOI: 10.1021/es5047155
Environ. Sci. Technol. 2015, 49, 3435−3443

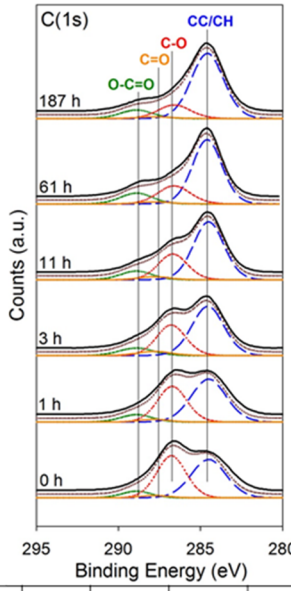

Sample	O:C	% CC/CH	% C-O	% C=O	% O-C=O
0 h	0.58	46	43	2	7
1 h	0.55	52	36	3	8
3 h	0.54	55	31	5	9
11 h	0.48	61	26	3	9
61 h	0.46	65	20	2	12
187 h	0.36	73	15	2	10

Figure 4. Spectral changes of air-equilibrated GO samples with sunlight exposure, showing XPS spectra of phototransformed GO products. The table shows changes in oxygen-to-carbon atom ratio and functional groups of GO samples during irradiation.

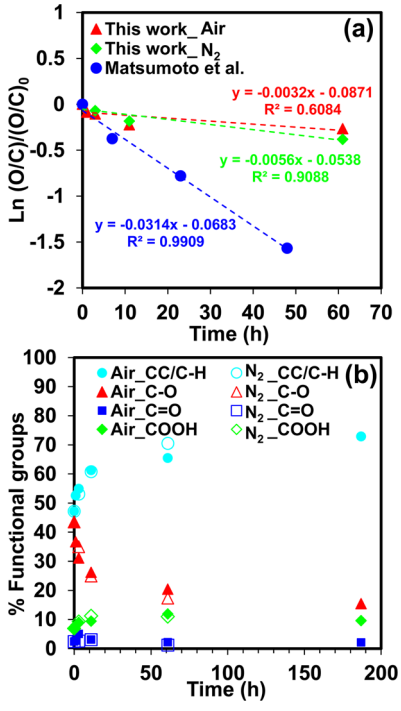

Figure 5. Time course changes of (a) the oxygen-to-carbon ratio (O/C) and (b) surface functional groups in air- and N_2-saturated GO samples under sunlight exposure. Data labeled as Matsumoto et al. are literature data generated with a 500 W xenon lamp in quartz vessels.[23]

0.0032 ± 0.0048 h^{-1} (±95% CI) with continued irradiation to 61 h. The inhomogeneous photoreaction behavior observed by XPS is consistent with CO_2 formation (Figure 2a), light absorbance (Figure 2b), I_D/I_G ratio measured by Raman (Figure S5, Supporting Information), and AFM size (Figure S6, Supporting Information) evolutions. Indeed, all of these various analytical measurements exhibit a similar kinetic profile, with the most significant changes occurring during the initial 10 h of irradiation, followed by little or no changes thereafter. These observation are attributed to the fact that intermediate photoproducts have significantly reduced photoreactivity from pristine GO.

In comparison to a study by Matsumoto et al. (O/C = 0.10 after 48 h) [$k_{obs} = 0.0314 \pm 0.0092$ h^{-1} (±95% CI), $R^2 = 0.99$],[23] Figure 5 also shows that our GO photoreduction rates are about 1 order of magnitude less with photoproducts having significant remaining oxygen-containing functionalities (O/C = 0.37), even after extended irradiation for 187 h. The discrepancy could be attributed to the irradiation conditions used earlier (i.e., 500 W xenon lamp in quartz reaction vessels) that involved energetic short wavelength light ($\lambda < 280$ nm) not present in the spectrum of the simulated solar light used here (i.e., 280−700 nm, 750 W). This suggests that additional photoreaction pathways likely occur under irradiation involving a shorter wavelength ($\lambda < 280$ nm) of light.

Figure 5b indicates that the rate of change in specific oxygen-containing functionalities also follows the initially rapid-then-slow pattern as a function of increasing irradiation time and that the concentration of each oxygen-containing functional group remains relatively stable with extended irradiation. The change in each functional group also does not closely follow the pseudo-first-order kinetics (as judged by R^2, Table S1, Supporting Information).

Considered with the photoproduct analysis, the kinetic data support the idea that photofragmentation of GO is rapid, producing reduced photoproducts similar to rGO that are significantly smaller in size as compared to the parent GO. However, once formed, these reduced photoproducts are much more resistant to further phototransformations as compared to GO (see Scheme 1).

Effect of O_2 Level (Air vs N_2 Purge). Figures S1a,b (Supporting Information) shows how the UV−visible spectra of GO evolve as a function of irradiation time. As absorbance values of irradiated samples also contain the absorbance of unreacted GO, we use difference spectra (Figure S1c,d, Supporting Information) in which the absorbance of parent GO is subtracted from absorbance values of irradiated samples to better represent absorbance values of photoproducts formed. The difference spectra reveal the appearance of a new absorbance peak at ~280 nm (Δ absorbance at 280 nm) indicative of the photoproducts formed.

Figure 2 indicates that CO_2 formation (Figure 2a) and light absorbance changes at 280 nm (inset in Figure 2b) are similar in both samples within the first 10 h. However, with continued irradiation, the CO_2 level in the air-saturated samples increases at a slower rate and eventually reaches a plateau, while CO_2 formation in N_2-saturated samples ceases altogether. Similarly, the UV−vis data of air- and N_2- equilibrated samples show distinct differences at longer irradiation times. During this period, absorbance in the air-saturated samples stops increasing and drops to a steady value five times smaller than N_2-saturated samples. Upon extended irradiation, Δ absorbance in N_2-saturated samples continues to increase until it reaches a plateau. These results are indicative of the buildup of more light-absorbing material in N_2-saturated systems. However, hydrodynamic sizes are similar for air- or N_2-saturated samples

DOI: 10.1021/es5047155
Environ. Sci. Technol. 2015, 49, 3435−3443

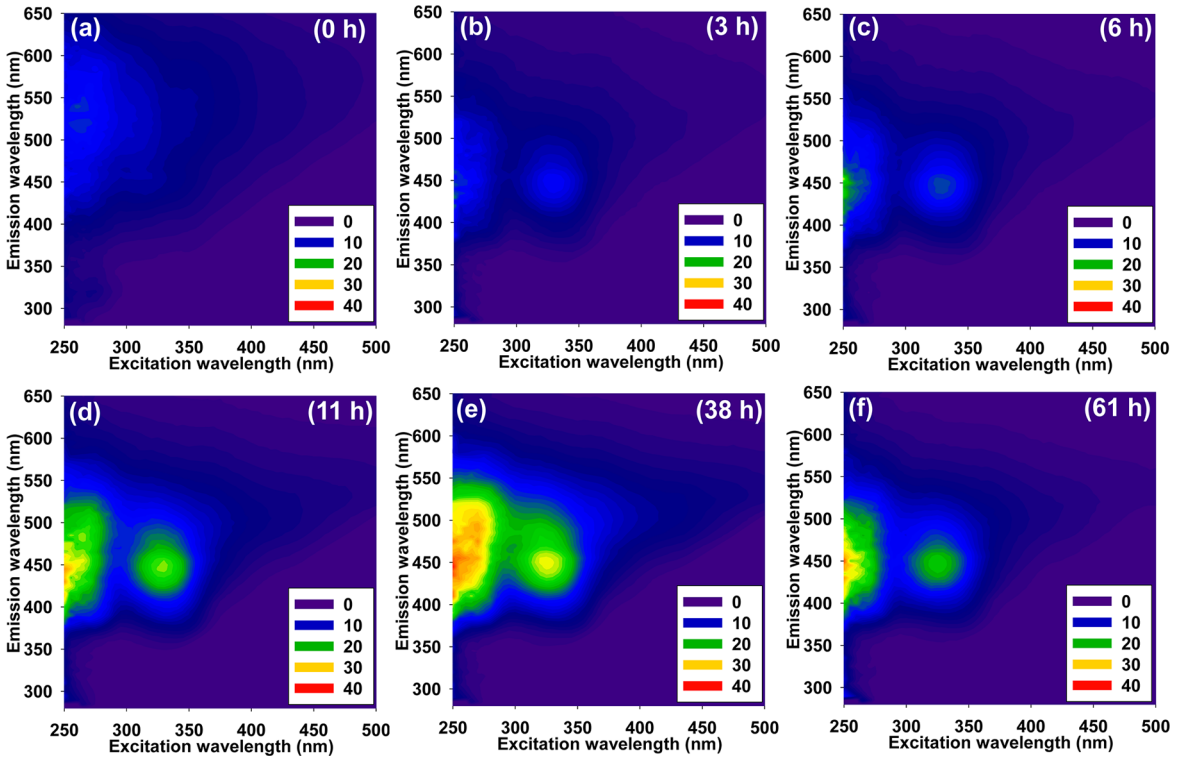

Figure 6. Excitation−emission matrices (EEM) characterizing the photoluminescence property of air-equilibrated GO samples before and after sunlight exposure. The intensity units are quinine sulfate equivalents and corrected for the inner filter effect.

over the entire course of irradiation (data not shown). We interpret this difference to be a result of the accumulation of LMW species (see Figure 3), not detectable by DLS, in N_2-purged systems that are generated during the initial and rapid fragmentation of GO. We postulate that in air-equilibrated systems these LMW species are converted into CO_2 accounting for the increase in CO_2 production observed at longer irradiation times in Figure 2a for air-equilibrated systems.

XPS analysis indicated that there was little difference in the nature or rate of the functional group changes observed between air and N_2 samples. We hypothesize the lack of difference (Figure 5b) between air and N_2 purged systems to be a consequence of the volatility of these LMW species formed during the initial photochemical transformation of GO could not survive freeze-drying and the ultrahigh vacuum environment required for XPS analysis. This would explain why there are differences in the CO_2 yield and UV−visible spectra between aerobic and anaerobic conditions at long irradiation times in the absence of any differences in XPS data.

Photoluminescence (PL) Characteristics. Recent studies indicate that GO is photoluminescent and that the PL represents the radiative electron−hole pair recombination. Consequently, the PL energy can be used to characterize the band gaps of electron transitions responsible for the PL.[3,37−39] Figure 6a indicates that parent GO exhibits an inhomogeneously broadened PL band in the range of 360−650 nm, with a maximum at ∼540 nm (2.30 eV) and excitation at 275 nm. The broad PL band of GO suggests that various electronic states are involved. The longer emission wavelength part of the PL band may arise from the relaxation of low-energy electronic states localized on specific oxygen functionality sites.[38] We believe that Figure 6 represents the first time the dynamic PL evolution of GO has been reported under photochemical conditions.

Upon irradiation there is a rapid decrease in oxygen functionalities and size in the reduced graphene oxide species (Figure 4) and as a result the PL band blue shifts to 380−550 nm, centered at ∼450 nm (2.76 eV) (Figure 6b). Initial irradiation also creates new electronic transitions with a PL band centered at 450 nm with excitation at 325 nm. The initial stages of photolysis are also characterized by an increase in PL intensity (Figure 6a−d) that we attribute to the removal of oxygen-containing functionalities, which act as efficient trap sites for electrons[40] and therefore reduce radiative electron relaxation (i.e., PL intensity).

As irradiation continues, the PL intensity starts to decrease (Figure 6f), although the PL wavelength characteristics remain largely unchanged. A similar evolution in the PL characteristics of GO have been reported previously after reaction with hydrazine (a strong reductant). This was attributed to delocalization of electron−hole pairs to nonradiative recombination centers, because extensive reduction leads to interconnectivity of sp^2 carbon domains.[3,41]

Recent work investigated mechanisms of GO photolysis in the aqueous phase: Gengler et al. suggested hydrated electrons (e_{aq}^-) generated from H_2O ionization under 266 nm UV (photon energy = 4.6 eV) laser pulse irradiation are responsible for GO photoreduction, by showing a two-photon process that overcomes the threshold energy of 6.5 eV for water ionization.[24] The two-photon process, however, usually requires energetic light sources such as laser pulses irrelevant to sunlight conditions in our study and it has been established that aqueous photoreactions mediated by laser pulses cannot predict those in natural systems.[42] The likely difference in reaction mechanisms is also supported by the differences in

DOI: 10.1021/es5047155
Environ. Sci. Technol. 2015, 49, 3435−3443

XPS data we observed, compared to previous studies conducted at lower wavelengths (Figure 5).

Assuming GO behaves like a photoreactive semiconductor,[3,23,38,43−46] photoreactions in our system could involve reactions mediated by electron−hole pair separation within GO. Indeed, our experimental observations (i.e., concurrent oxidation and reduction of GO, O_2-dependency, PL data, and H_2O_2 formation) are broadly consistent with an electron−hole pair-mediated process. Thus, the co-occurrence of oxidative (valence band holes, h_{vb}^+) and reductive (conduction band electron, e_{aq}^-) transients agrees with concurrent GO oxidation and reduction (disproportionation). The fact that the initial reaction (<10 h) is insensitive to O_2 could be attributed to strong e_{aq}^--trapping by the sites occupied by the oxygen-containing functional groups most abundant on parent GO. Moreover, we believe that e_{aq}^--trapping events by oxygen-containing functional groups contributes to the reduction of GO that occurs during the initial period of irradiation (Figure 5b). As the irradiation time continues and e_{aq}^- trapping by the oxygen functional groups decreases, the relative importance of dissolved oxygen becomes more apparent because e_{aq}^- can also be scavenged by O_2 ($k_{O2,eaq} = 1.6 \times 10^{10}$ M^{-1} s^{-1}).[47,48] The electron−hole pair separation efficiency would therefore be enhanced by e_{aq}^- trapping, enhancing oxidative reactions affected by h_{vb}^+, such as CO_2 formation that continues for longer (>10 h) irradiation times in air-equilibrated samples (Figure 2a). Such a scenario would predict that the effect of O_2 would become more important once the trap sites associated with the oxygen containing functional groups are removed, consistent with our observations. We also measured the formation of submillimolar H_2O_2 (data not shown) that supports the e_{aq}^- formation because e_{aq}^- scavenging by O_2 would result in the formation of superoxide that disproportionates to H_2O_2. Although our results are broadly consistent with electron−hole pair-mediated photoreactions, further studies are needed to confirm the proposed mechanisms.

Environmental Implications. GO has emerged in a range of applications. When it makes its way into ecosystems, environmental factors play a role in controlling its fate, transport, and ecotoxicity. Our work suggests that direct photolysis under sunlight conditions will rapidly remove GO by photochemically converting it to CO_2, fragmented photoproducts similar to rGO, and LMW species. However, GO photoproducts are markedly less photoreactive and persist even after exposure equivalent to ∼2 months of natural sunlight. This suggests that end-products are likely to accumulate in the environment and probably could only be removed by environmental processes other than direct photolysis. Significant changes in the physicochemical properties of GO with sunlight exposure suggests that the transformed products will have transport and eco-toxicological effects distinct from those of the parent GO.

■ ASSOCIATED CONTENT

Supporting Information

Additional information on experimental procedures for oxygen level studies, CO_2 measurement, and photoproduct preparation and characterization using mass spectrometry, GC, XPS, ATR-IR, DLS, fluorescence, and AFM, UV−visible absorbance spectra and difference spectra of air- and N_2-saturated samples, XPS, ATR-IR and Raman spectra of N_2-saturated samples, AFM size changes, pseudo-first rates for individual functional group changes, as well as I_D/I_G ratio evolution. This material is available free of charge via the Internet at http://pubs.acs.org.

■ AUTHOR INFORMATION

Corresponding Authors

*W.-C. Hou. Phone: +886 62757575 ext. 65842. Fax: +886 6 2752790. E-mail: whou@mail.ncku.edu.tw.

*R. G. Zepp. Phone: (706) 355-8117. Fax: (706) 355-8007. E-mail: zepp.richard@epa.gov.

Notes

The authors declare no competing financial interest.

■ ACKNOWLEDGMENTS

This paper has been reviewed in accordance with the U.S. Environmental Protection Agency's (U.S. EPA) peer and administrative review policies and approved for publication. Mention of trade names or commercial products does not constitute an endorsement or recommendation for use by the U.S. EPA. Financial support provided by the Ministry of Science and Technology (MOST) of Taiwan (for Hou) under grant number MOST 103-2221-E-006-015-MY3 is acknowledged. D.H.F. acknowledges financial support by the U.S. EPA under grant R834858.

■ REFERENCES

(1) Zhu, Y.; Murali, S.; Cai, W.; Li, X.; Suk, J. W.; Potts, J. R.; Ruoff, R. S. Graphene and graphene oxide: Synthesis, properties, and applications. *Adv. Mater.* **2010**, *22*, 3906−3924.

(2) Novoselov, K. S.; Fal'ko, V. I.; Colombo, L.; Gellert, P. R.; Schwab, M. G.; Kim, K. A roadmap for graphene. *Nature* **2012**, *490*, 192−200.

(3) Eda, G.; Lin, Y.-Y.; Mattevi, C.; Yamaguchi, H.; Chen, H.-A.; Chen, I.-S.; Chen, C.-W.; Chhowalla, M. Blue photoluminescence from chemically derived graphene oxide. *Adv. Mater.* **2010**, *22*, 505−509.

(4) Dreyer, D. R.; Park, S.; Bielawski, C. W.; Ruoff, R. S. The chemistry of graphene oxide. *Chem. Soc. Rev.* **2010**, *39*, 228.

(5) Gao, W.; Alemany, L. B.; Ci, L.; Ajayan, P. M. New insights into the structure and reduction of graphite oxide. *Nat. Chem.* **2009**, *1*, 403−408.

(6) Pei, S.; Cheng, H.-M. The reduction of graphene oxide. *Carbon* **2012**, *50*, 3210−3228.

(7) Stankovich, S.; Dikin, D. A.; Piner, R. D.; Kohlhaas, K. A.; Kleinhammes, A.; Jia, Y.; Wu, Y.; Nguyen, S. T.; Ruoff, R. S. Synthesis of graphene-based nanosheets via chemical reduction of exfoliated graphite oxide. *Carbon* **2007**, *45*, 1558−1565.

(8) Salas, E. C.; Sun, Z.; Lüttge, A.; Tour, J. M. Reduction of graphene oxide via bacterial respiration. *ACS Nano* **2010**, *4*, 4852−4856.

(9) Williams, G.; Seger, B.; Kamat, P. V. TiO_2-Graphene nanocomposites. UV-assisted photocatalytic reduction of graphene oxide. *ACS Nano* **2008**, *2*, 1487−1491.

(10) Akhavan, O.; Ghaderi, E. Toxicity of graphene and graphene oxide nanowalls against bacteria. *ACS Nano* **2010**, *4*, 5731−5736.

(11) Liu, S.; Zeng, T. H.; Hofmann, M.; Burcombe, E.; Wei, J.; Jiang, R.; Kong, J.; Chen, Y. Antibacterial activity of graphite, graphite oxide, graphene oxide, and reduced graphene oxide: Membrane and oxidative stress. *ACS Nano* **2011**, *5*, 6971−6980.

(12) Perreault, F.; Tousley, M. E.; Elimelech, M. Thin-film composite polyamide membranes functionalized with biocidal graphene oxide nanosheets. *Environ. Sci. Technol. Lett.* **2013**, *1*, 71−76.

(13) Ahmed, F.; Rodrigues, D. F. Investigation of acute effects of graphene oxide on wastewater microbial community: A case study. *J. Hazard. Mater.* **2013**, *256−257*, 33−39.

DOI: 10.1021/es5047155
Environ. Sci. Technol. 2015, 49, 3435−3443

(14) Begum, P.; Ikhtiari, R.; Fugetsu, B. Graphene phytotoxicity in the seedling stage of cabbage, tomato, red spinach, and lettuce. *Carbon* **2011**, *49*, 3907−3919.
(15) Guo, X.; Dong, S.; Petersen, E. J.; Gao, S.; Huang, Q.; Mao, L. Biological uptake and depuration of radio-labeled graphene by *Daphnia magna*. *Environ. Sci. Technol.* **2013**, *47*, 12524−12531.
(16) Chowdhury, I.; Duch, M. C.; Mansukhani, N. D.; Hersam, M. C.; Bouchard, D. Colloidal properties and stability of graphene oxide nanomaterials in the aquatic environment. *Environ. Sci. Technol.* **2013**, *47*, 6288−6296.
(17) Chowdhury, I.; Duch, M. C.; Mansukhani, N. D.; Hersam, M. C.; Bouchard, D. Deposition and release of graphene oxide nanomaterials using a quartz crystal microbalance. *Environ. Sci. Technol.* **2014**, *48*, 961−969.
(18) Lanphere, J. D.; Rogers, B.; Luth, C.; Bolster, C. H.; Walker, S. L. Stability and transport of graphene oxide nanoparticles in groundwater and surface water. *Environ. Eng. Sci.* **2014**, *31*, 350−359.
(19) Wu, L.; Liu, L.; Gao, B.; Muñoz-Carpena, R.; Zhang, M.; Chen, H.; Zhou, Z.; Wang, H. Aggregation kinetics of graphene oxides in aqueous solutions: Experiments, mechanisms, and modeling. *Langmuir* **2013**, *29*, 15174−15181.
(20) Qi, Z.; Zhang, L.; Wang, F.; Hou, L.; Chen, W. Factors controlling transport of graphene oxide nanoparticles in saturated sand columns. *Environ. Toxicol. Chem.* **2014**, *33*, 998−1004.
(21) Kotchey, G. P.; Allen, B. L.; Vedala, H.; Yanamala, N.; Kapralov, A. A.; Tyurina, Y. Y.; Klein-Seetharaman, J.; Kagan, V. E.; Star, A. The enzymatic oxidation of graphene oxide. *ACS Nano* **2011**, *5*, 2098−2108.
(22) Gurunathan, S.; Han, J. W.; Eppakayala, V.; Kim, J.-H. Microbial reduction of graphene oxide by *Escherichia coli*: A green chemistry approach. *Colloids Surf., B* **2013**, *102*, 772−777.
(23) Matsumoto, Y.; Koinuma, M.; Ida, S.; Hayami, S.; Taniguchi, T.; Hatakeyama, K.; Tateishi, H.; Watanabe, Y.; Amano, S. Photoreaction of graphene oxide nanosheets in water. *J. Phys. Chem. C* **2011**, *115*, 19280−19286.
(24) Gengler, R. Y. N.; Badali, D. S.; Zhang, D.; Dimos, K.; Spyrou, K.; Gournis, D.; Miller, R. J. D. Revealing the ultrafast process behind the photoreduction of graphene oxide. *Nat. Commun.* **2013**, *4*.
(25) McDonald, M. P.; Eltom, A.; Vietmeyer, F.; Thapa, J.; Morozov, Y. V.; Sokolov, D. A.; Hodak, J. H.; Vinodgopal, K.; Kamat, P. V.; Kuno, M. Direct observation of spatially heterogeneous single-layer graphene oxide reduction kinetics. *Nano Lett.* **2013**, *13*, 5777−5784.
(26) Lester, Y.; Sharpless, C. M.; Mamane, H.; Linden, K. G. Production of photo-oxidants by dissolved organic matter during UV water treatment. *Environ. Sci. Technol.* **2013**, *47*, 11726−11733.
(27) Hummers, W. S.; Offeman, R. E. Preparation of graphitic oxide. *J. Am. Chem. Soc.* **1958**, *80*, 1339−1339.
(28) Marcano, D. C.; Kosynkin, D. V.; Berlin, J. M.; Sinitskii, A.; Sun, Z.; Slesarev, A.; Alemany, L. B.; Lu, W.; Tour, J. M. Improved synthesis of graphene oxide. *ACS Nano* **2010**, *4*, 4806−4814.
(29) Fan, Z.-J.; Kai, W.; Yan, J.; Wei, T.; Zhi, L.-J.; Feng, J.; Ren, Y.; Song, L.-P.; Wei, F. Facile synthesis of graphene nanosheets via Fe reduction of exfoliated graphite oxide. *ACS Nano* **2011**, *5*, 191−198.
(30) Li, D.; Müller, M. B.; Gilje, S.; Kaner, R. B.; Wallace, G. G. Processable aqueous dispersions of graphene nanosheets. *Nat. Nano* **2008**, *3*, 101−105.
(31) Zhou, X.; Zhang, Y.; Wang, C.; Wu, X.; Yang, Y.; Zheng, B.; Wu, H.; Guo, S.; Zhang, J. Photo-Fenton reaction of graphene oxide: A new strategy to prepare graphene quantum dots for DNA cleavage. *ACS Nano* **2012**, *6*, 6592−6599.
(32) Bai, H.; Jiang, W.; Kotchey, G. P.; Saidi, W. A.; Bythell, B. J.; Jarvis, J. M.; Marshall, A. G.; Robinson, R. A. S.; Star, A. Insight into the mechanism of graphene oxide degradation via the photo-Fenton reaction. *J. Phys. Chem. C* **2014**, *118*, 10519−10529.
(33) Ferrari, A. C.; Robertson, J. Interpretation of Raman spectra of disordered and amorphous carbon. *Phys. Rev. B* **2000**, *61*, 14095−14107.
(34) Ferrari, A. C.; Basko, D. M. Raman spectroscopy as a versatile tool for studying the properties of graphene. *Nat. Nanotechnol.* **2013**, *8*, 235−246.
(35) Lucchese, M. M.; Stavale, F.; Ferreira, E. H. M.; Vilani, C.; Moutinho, M. V. O.; Capaz, R. B.; Achete, C. A.; Jorio, A. Quantifying ion-induced defects and Raman relaxation length in graphene. *Carbon* **2010**, *48*, 1592−1597.
(36) Jorio, A.; Martins Ferreira, E. H.; Cancado, L. G.; Achete, C. A.; Capaz, R. B. Measuring Disorder in Graphene with Raman Spectroscopy. In *Physics and Applications of Graphene - Experiments*; Mikhailov, S., Ed.; InTech: Rijeka, Croatia, 2011.
(37) Novoselov, K. S.; Geim, A. K.; Morozov, S. V.; Jiang, D.; Zhang, Y.; Dubonos, S. V.; Grigorieva, I. V.; Firsov, A. A. Electric field effect in atomically thin carbon films. *Science* **2004**, *306*, 666−669.
(38) Chien, C.-T.; Li, S.-S.; Lai, W.-J.; Yeh, Y.-C.; Chen, H.-A.; Chen, I.-S.; Chen, L.-C.; Chen, K.-H.; Nemoto, T.; Isoda, S.; et al. Tunable photoluminescence from graphene oxide. *Angew. Chem., Int. Ed.* **2012**, *51*, 6662−6666.
(39) Shang, J.; Ma, L.; Li, J.; Ai, W.; Yu, T.; Gurzadyan, G. G. The Origin of Fluorescence from Graphene Oxide. *Sci. Rep.* **2012**, *2*.
(40) Kaniyankandy, S.; Achary, S. N.; Rawalekar, S.; Ghosh, H. N. Ultrafast relaxation dynamics in graphene oxide: Evidence of electron trapping. *J. Phys. Chem. C* **2011**, *115*, 19110−19116.
(41) Cao, L.; Meziani, M. J.; Sahu, S.; Sun, Y.-P. Photoluminescence properties of graphene versus other carbon nanomaterials. *Acc. Chem. Res.* **2013**, *46*, 171−180.
(42) Wang, W.; Zafiriou, O. C.; Chan, I.-Y.; Zepp, R. G.; Blough, N. V. Production of hydrated electrons from photoionization of dissolved organic matter in natural waters. *Environ. Sci. Technol.* **2007**, *41*, 1601−1607.
(43) Yeh, T.-F.; Syu, J.-M.; Cheng, C.; Chang, T.-H.; Teng, H. Graphite oxide as a photocatalyst for hydrogen production from water. *Adv. Funct. Mater.* **2010**, *20*, 2255−2262.
(44) Yeh, T.-F.; Chan, F.-F.; Hsieh, C.-T.; Teng, H. Graphite oxide with different oxygenated levels for hydrogen and oxygen production from water under illumination: The band positions of graphite oxide. *J. Phys. Chem. C* **2011**, *115*, 22587−22597.
(45) Jiang, X.; Nisar, J.; Pathak, B.; Zhao, J.; Ahuja, R. Graphene oxide as a chemically tunable 2-D material for visible-light photocatalyst applications. *J. Catal.* **2013**, *299*, 204−209.
(46) Hsu, H.-C.; Shown, I.; Wei, H.-Y.; Chang, Y.-C.; Du, H.-Y.; Lin, Y.-G.; Tseng, C.-A.; Wang, C.-H.; Chen, L.-C.; Lin, Y.-C.; et al. Graphene oxide as a promising photocatalyst for CO_2 to methanol conversion. *Nanoscale* **2012**, *5*, 262−268.
(47) Zepp, R. G.; Braun, A. M.; Hoigne, J.; Leenheer, J. A. Photoproduction of hydrated electrons from natural organic solutes in aquatic environments. *Environ. Sci. Technol.* **1987**, *21*, 485−490.
(48) Buxton, G. V.; Greenstock, C. L.; Helman, W. P.; Ross, A. B. Critical review of rate constants for reactions of hydrated electrons, hydrogen atoms and hydroxyl radicals (OH/O^- in aqueous solution. *J. Phys. Chem. Ref. Data* **1988**, *17*, 513−886.

DOI: 10.1021/es5047155
Environ. Sci. Technol. 2015, 49, 3435−3443